IRDM: A generative diffusion model for indoor radio map interpolation

Kehai Qiu, Stefanos Bakirtzis, Ian Wassell
Dept. of Computer Science and Technology
University of Cambridge
Cambridge, United Kingdom
kq218@cam.ac.uk, ssb45@cam.ac.uk, ijw24@cam.ac.uk

Hui Song, Kan Lin, Jie Zhang
Ranplan Wireless
Hui.Song@ranplanwireless.com
Kan.Lin@ranplanwireless.com
Jie.Zhang@ranplanwireless.com

***Abstract*—This article proposes a novel methodology for interpolating path-loss radio maps, which are vital for comprehending signal distribution and hence planning indoor wireless networks. The approach employs generative diffusion models and proves to be highly effective in generating accurate radio maps with only a small number of measurements. The experimental outcomes demonstrate an average root-mean-square error of 4.23 dB using only 10 percent of the reference points, highlighting the ability of the generative diffusion model to achieve significant interpolation accuracy in radio map generation.**

***Index Terms*—Radio map interpolation, path loss calculation, diffusion model, ray tracing**

I. INTRODUCTION

The next generation of networks, including 5G and beyond, will need to use dynamic spectrum sharing and power domain multiple access to handle the rising amount of mobile data traffic [1]. To make this possible, we need to develop more accurate methods of estimating the radio environment, including signal strength and spectrum availability in the proposed service areas.

Path loss information indicating the signal quality in the proposed service area owing to different access points (APs) is an essential component of network deployment planning in an indoor radio environment. Therefore, acquiring a predicted indoor path loss map (IPM) or received signal strength (RSS) map prior to the deployment of APs is essential as it allows for accurate estimation of signal strength and coverage within buildings and helps in the placement of APs. In addition, an accurate IPM can enable applications such as precise indoor localisation [2], cognitive radio networks [3], and mobile robots [4].

Obtaining an accurate IPM can be a time-consuming and labor-intensive process, as it requires taking measurements at numerous reference points (RPs) in the proposed service area and the installation of test APs. To address this issue, various techniques have been proposed, such as interpolation methods that predict the IPM based on measurements taken at reference points, and generative methods that predict the IPM without the use of RPs.

Racko et al. [5] employed linear and Delaunay interpolation techniques for radio map generation. By measuring RSS at designated positions, they were able to calculate the complete RSS through the use of two distinct interpolation methods. Moreover, [6] adopts an image-driven approach, which treats radio propagation data as an image and estimates the RSS geographical distribution using image processing techniques. Through path loss regression, the proposed deep learning (DL) framework converts the spatial interpolation problem into a shadowing adjustment problem, which is then addressed by a neural network (NN). Additionally, a gradual training method is used for NN stability, in which the encoding/decoding blocks are trained separately.

In [7], Jan et al. computed RSS values at unobserved locations with kriging, creating an expanded RSS database at a very small number of RPs in addition to RSS measurements alone. By increasing the size of the database, i.e., the number of basic RPs and kriging RPs, the interpolation error can be reduced. Similarly, in [8], RSS values for interpolated points are calculated using a Euclidean distance linear basis, multi-quadratic, thin-plate spline, and poly-harmonic spline functions. However, the method employed in the aforementioned study had an interpolated area of limited dimensions due to the proximity of the RPs to the AP and the restricted coverage area.

Ray tracing or ray launching is a computational technique extensively utilized in the simulation of radio maps to model the propagation of electromagnetic waves in complex environments [9]. The method involves tracing the path of rays emanating from a transmitter as they interact with various elements within the environment, including reflection, refraction, and diffraction. By accurately capturing these interactions, ray tracing provides a reliable means to estimate radio signal characteristics such as strength, delay, and angle of arrival.

Generative models make use of the same information required for ray tracing (environment and transmitter information) and generate the IPM accordingly. Most of the existing indoor propagation models use simple multilayer perceptrons (MLPs) to generate IPMs [10], [11]. Some recent approaches leverage more complex networks, for example, Ratnam et at. [12] applied U-Net-like convolutional neural networks to path loss prediction problems and reduced prediction time by 40 to 1000 times in comparison to industry prevalent methods such as ray-tracing. Stefanos et al. [13] utilized a modified version of the U-Net architecture and stacked dilated convolutions to improve the accuracy of prediction by 2-4dB compared with [12]. However, these works do not utilize path loss measurements to calibrate the proposed models.

Considering the aforementioned challenges, we propose a novel approach that employs generative diffusion models (GDM) [14] to interpolate incomplete indoor path loss maps using a limited number of RPs. By leveraging the advantages of generative models and interpolation methods, our approach facilitates the development of highly precise and comprehensive indoor path loss maps that incorporate building information with an accuracy that is not constrained by the number of RPs. This interpolation method is expected to provide valuable insights for wireless network planning and deployment.

The major contributions of this paper can be summarized as follows:

1. As far as we are aware, our proposed approach represents the first attempt to utilize a GDM for the task of interpolating incomplete indoor path loss maps. In addition, we introduce unique data processing methods that enable the generative diffusion model to effectively capture the underlying signal characteristics and generate accurate radio maps.

2. We propose a multi-stage training strategy along with an online data augmentation method for improving the stability and accuracy of the training phase. Furthermore, we introduce an online data augmentation method to enhance the training dataset and improve the generalization performance of the model.

II. Data Collection and Data Pre-Processing

A. Data Collection

The dataset comprises 10,000 samples, each representing the output of an indoor radio propagation simulation having a spatial resolution of 0.5m. To train our model, we simulated path loss for multiple indoor environments, including the one illustrated in Fig.1, using 3D-ray-tracing software (Ranplan Professional) [15]. Due to the exponential increase in computational complexity associated with 3D ray-tracing algorithms, we have opted not to collect radio map data at a higher resolution. This decision is further justified by the considerable time required to process extensive datasets. The sample grid size for each simulation varies based on the building size, and we cropped it to 64×64 pixels for data augmentation purposes. The grayscale value of each pixel represents the path loss, which is the difference between the transmitting signal power and the received signal strength measured in decibels (dB) in a 0.5×0.5 m^2 area

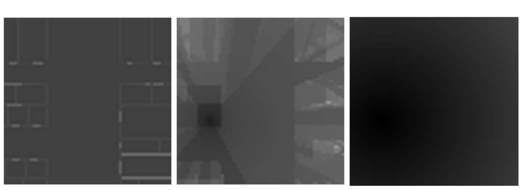

Fig. 1. Example region showing three layers, i.e., geometry (left), IPM (mid), positional encoding layer (right)

B. Data Post-Processing

In our dataset, each region is processed to produce two equal-sized 2D images, both consisting of three layers. The first layer and the third layer in both the training region and the target are identical, as they only contain information about the location of the APs and region geometry. The only difference between the two images lies in the second layer, referred to as the IPM layer, which records the path loss value for each grid point based on a 3D ray tracing simulation.

These three layers are incorporated into separate channels, as illustrated in Fig. 1. The geometry layer represents the locations and types of indoor materials using appropriate values for the various materials. The positional layer offers a distance reference from the AP, using a 2D Gaussian kernel.

$$G(x,y) = \frac{1}{2\pi\sigma^2} e^{-\dfrac{x^2+y^2}{2\sigma^2}} \tag{1}$$

where x and y represent the distance from the transmitter in the two axes, and σ is the standard deviation of the Gaussian distribution. For our experiments, σ was set to 3. This formula generates a surface with concentric circles that follow a Gaussian distribution from the center of the AP, emphasizing location information and avoiding a sparse matrix in this layer.

The second layer represents the IPM layer, with path loss calculated through ray tracing in the simulated indoor environment. We utilized omnidirectional antennas for transmission and reception, with a transmitting frequency of 2.4 GHz. The AP's transmitting power is 30 dBm at an antenna height of 3m above the floor level, and the receive antenna is positioned at a height of 1.5m above the floor level.

The training set was generated using an online data augmentation technique, which involves randomly selecting a specific fraction of RPs from the IPM layer and appending them to the geometry and positional encoding layers during the training phase. Additionally, the sampled map and target were rotated randomly by 90°, 180°, or 270° for data enrichment purposes.

III. Radio map generation

A. Background on Generative diffusion model

Deep generative diffusion models such as the denoising diffusion probabilistic models (DDPM) [16] have gained prominence in the field of image processing due to their exceptional ability to generate high-quality images through a noise-to-signal process. These models employ a diffusion process that gradually refines a noisy input, allowing for better control and more effective removal of unwanted artifacts. Their state-of-the-art performance in tasks such as image synthesis, restoration, and generation has made them a subject of extensive study and application.

Figure 2 illustrates how a DDPM model is constructed for the image-denoising task, which can be seen to comprise two intertwined processes. The first process, known as the forward diffusion process, progressively injects noise into the original data distribution through a sequence of time steps, eventually converting it into a more straightforward to handle Gaussian distribution after a predetermined number of steps. The second process also referred to as the denoising or reverse process seeks to recover the initial data from the noise-affected samples by leveraging a neural network for parameterization.

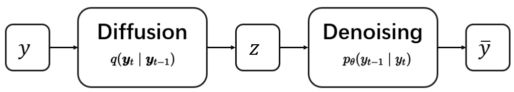

Fig. 2. The diffusion model applies the forward diffusion process q to the original data y in a gradual manner, adding noise until it matches a known noise distribution z. Then, using a reversed inference process function p, it reverses each step of the sampling process to produce a denoised image $\overline{y}$.

DDPMs [**?**], [17] are latent variable models that have a form similar to that illustrated in Fig.3,

$$
\begin{aligned}
& p_\theta\left(\boldsymbol{y}_0\right)=\int p_\theta\left(\boldsymbol{y}_{0: T}\right) \mathrm{d} \boldsymbol{y}_{1: T} \quad \text { where } \\
& p_\theta\left(\boldsymbol{y}_{0: T}\right):=p_\theta\left(\boldsymbol{y}_T\right) \prod_{t=1}^T p_\theta^{(t)}\left(\boldsymbol{y}_{t-1} \mid \boldsymbol{y}_t\right)
\end{aligned}
$$

and $y_1, ..., y_t$ are latent variables in the same sample space as y_0. The parameters θ are learned to fit the data distribution $q(y_0)$ by maximizing a variational lower bound:

$$
\begin{aligned}
& \max_\theta \mathbb{E}_{q\left(\boldsymbol{y}_0\right)}\left[\log p_\theta\left(\boldsymbol{y}_0\right)\right] \quad \leq \\
& \max_\theta \mathbb{E}_{q\left(\boldsymbol{y}_0, \boldsymbol{y}_1, \ldots, \boldsymbol{y}_T\right)}\left[\log p_\theta\left(\boldsymbol{y}_{0: T}\right)-\log q\left(\boldsymbol{y}_{1: T} \mid \boldsymbol{y}_0\right)\right]
\end{aligned}
$$

where $q\left(\boldsymbol{y}_{1: T} \mid \boldsymbol{y}_0\right)$ is some inference distribution over the latent variables.

DDPMs are learned with a fixed inference procedure, Ho et al. [17] considered the following Markov chain with Gaussian transitions parameterized by a decreasing sequence $\alpha_{1: T} \in (0,1]^T$

$$
\begin{aligned}
& q\left(\boldsymbol{y}_{1: T} \mid \boldsymbol{y}_0\right):=\prod_{t=1}^T q\left(\boldsymbol{y}_t \mid \boldsymbol{y}_{t-1}\right), \text { where } \\
& q\left(\boldsymbol{y}_t \mid \boldsymbol{y}_{t-1}\right):=\mathcal{N}\left(\sqrt{\frac{\alpha_t}{\alpha_{t-1}}} \boldsymbol{y}_{t-1},\left(1-\frac{\alpha_t}{\alpha_{t-1}}\right) \boldsymbol{I}\right)
\end{aligned}
$$

This process is characterized by its autoregressive nature, in which Gaussian noise is incrementally introduced to the image through a fixed Markov chain, represented by $q(\boldsymbol{y}t \mid \boldsymbol{y}t-1)$. In contrast, the denoising or reverse process focuses on the iterative restoration of an image from its noisy observation.

It is worth mentioning that, in the forward process,

$$
\begin{aligned}
q\left(\boldsymbol{y}_t \mid \boldsymbol{y}_0\right) & :=\int q\left(\boldsymbol{y}_{1: t} \mid \boldsymbol{y}_0\right) \mathrm{d} \boldsymbol{y}_{1:(t-1)} \\
& =\mathcal{N}\left(\boldsymbol{y}_t ; \sqrt{\alpha_t} \boldsymbol{y}_0,\left(1-\alpha_t\right) \boldsymbol{I}\right)
\end{aligned}
$$

therefore, we can express $\boldsymbol{y}_t$ as a linear combination of $\boldsymbol{y}_0$ and a noise variable ϵ:

$$
\boldsymbol{y}_t=\sqrt{\alpha_t} \boldsymbol{y}_0+\sqrt{1-\alpha_t} \epsilon, \quad \text { where } \quad \epsilon \sim \mathcal{N}(\mathbf{0}, \boldsymbol{I}).
$$

When we set α_t close to 0, $q\left(\boldsymbol{y}_t \mid \boldsymbol{y}_0\right)$ converges to a standard Gaussian for all $\boldsymbol{y}_0$, and it is thus natural to set $p_\theta\left(\boldsymbol{x}_T\right):=\mathcal{N}(\mathbf{0}, \boldsymbol{I})$.

Since all the conditionals are modeled as Gaussian with trainable mean function and fixed variances, the objective function can be simplified to:

$$
\begin{aligned}
& L_\gamma\left(\epsilon_\theta\right):=\sum_{t=1}^T \gamma_t \mathbb{E}_{\boldsymbol{y}_0} \sim q\left(\boldsymbol{y}_0\right), \\
& \epsilon_t \sim \mathcal{N}(\mathbf{0}, I)\left[\left\|\epsilon_\theta^{(t)}\left(\sqrt{\alpha_t} \boldsymbol{y}_0+\sqrt{1-\alpha_t} \epsilon_t\right)-\epsilon_t\right\|_2^2\right]
\end{aligned}
$$

where $\epsilon_\theta:=\left\{\epsilon_\theta^{(t)}\right\}_{t=1}^T$ is a neural denoising model with a set of T function, and θ represents the learnable parameters. The denoising model is trained to reverse this diffusion process by iteratively removing the noise in a series of steps. $\gamma:=\left[\gamma_1, \ldots, \gamma_T\right]$ is a vector of positive coefficients in the objective that depends on $\alpha_{1: T}$.

In [17], the objective with $\gamma=1$ is optimized instead to maximize the denoising performance of the trained model. For a trained model, $\boldsymbol{y}_0$ is generated by first sampling $\boldsymbol{y}_t$ based on the prior $p_\theta\left(\boldsymbol{y}_T\right)$, and then generating $\boldsymbol{y}_t-1$ iteratively. The value of T, the length of generative steps, is an important hyperparameter in DDPMs since a large T allows the reverse process to be close to a Gaussian distribution, thus modeling the generative process with Gaussian distributions becomes a good approximation.

B. Radio diffusion model

A conditional diffusion model [18] makes the denoising process conditional on an input signal, and further image-to-image diffusion models are conditional diffusion models of the form $p(\boldsymbol{y}|\boldsymbol{x})$ that leverage a dataset of input-output image pairs. Inspired by Saharia et al. [19], we have elected to apply diffusion models to the task of radio map generation. We hypothesize that the diffusion process, renowned for its capability to produce high-quality images through iterative refinements, could similarly enhance the fidelity and accuracy of radio maps. Given the model's proven effectiveness in complex image-based tasks, we believe it holds promise for addressing challenges inherent to large-scale, high-resolution radio map simulations.

In our study, we work with input-output image pairs in our synthetic dataset, where the data distribution $\boldsymbol{y}$ includes high-resolution (HR) images with complete IPMs and corresponding low-resolution (LR) images $\boldsymbol{x}$ using sampled IPM maps, as shown in Fig.4. The conditional distribution $p(\boldsymbol{y}|\boldsymbol{x})$ denotes a many-to-one mapping for LR to HR image conversion, meaning multiple source images can map to one target image. We aim to learn a parametric approximation of $p(\boldsymbol{y}|\boldsymbol{x})$, transforming a source image $\boldsymbol{y_t}$ with the condition $\boldsymbol{x}$ into a target image $\boldsymbol{y_0}$.

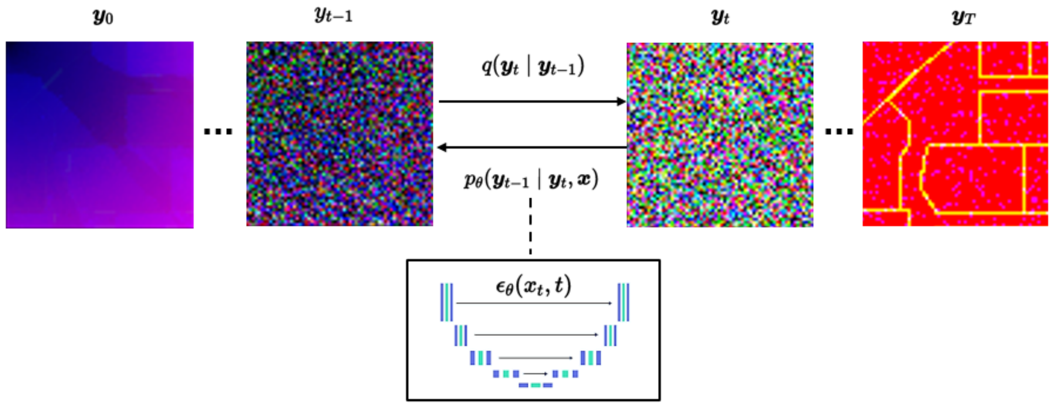

Fig. 3. Forward diffusion process q and reverse inference process p in radio diffusion model (RDM). The forward process q (left-to-right) incrementally introduces Gaussian noise to the target IPM, while the reverse process p (right-to-left) successively refines the target IPM based on the sampled IPM image x. ϵ_θ is a neural network that learns the denoising step.

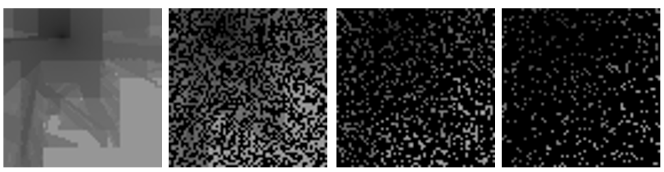

Fig. 4. Full IPM (left) and sampled IPMs (remainder) with sample ratio of 0.5, 0.2, 0.1 moving from left to right

To achieve this, we employ a conditional diffusion model known as the radio diffusion model (RDM), which is adapted from the SR3 model proposed by Saharia et al. [18] for image super-resolution.

Our RDM's architecture resembles U-Net in DDPM [17] with self-attention as the function ϵ_θ, and we reduce the number of residual blocks to two from the three used in SR3 to reduce processing time. Given geometry information as side information, and incomplete IPMs (either sampled IPMs or measurements), the goal of our model is to recover the full IPM.

Inference of RDM is conducted using the trained reverse process. The reverse process is designed to ensure that the prior distribution $p(y_T)$ closely approximates the interpolation procedure.

We train the models with T equal to 2000 using a mini-batch size of 16 for 2 million training steps. Overfitting is not observed during training, and thus we use the final model checkpoint at 2 million steps to report the final results. To optimize the models, we use a standard Adam optimizer with a fixed learning rate of 1e-4 and a linear learning rate warm-up schedule of 10k samples.

IV. Result and Analysis

Results of the IPM interpolation at various steps are depicted in Fig.3, where the sampled IPM is initially considered as a noisy, incomplete IPM, and then gradually denoised to achieve completeness.

To evaluate the performance of RDM we use the root-mean-squared error (RMSE) as is often employed for such tasks in [20] and is defined as:

$$RMSE = \sqrt{\frac{\sum_{n=1}^{N}\sum_{i=1}^{W}\sum_{j=1}^{H}\left(y_{(n)}(i,j) - \hat{y}_{(n)}(i,j)\right)^2}{NWH}} \quad (2)$$

where y and $\hat{y}$ are the full IPM and IPM after interpolation respectively, and N is the number of samples, W and H are the width and height of IPMs separately.

A. Training from scratch

To evaluate the performance of our model, we conducted three separate experiments and trained our model with sample ratios of 0.1, 0.2, and 0.5, respectively, without using pre-trained weights. Subsequently, we tested the trained models with unknown geometries using the sampled IPM with the same sample ratio as that used during training.

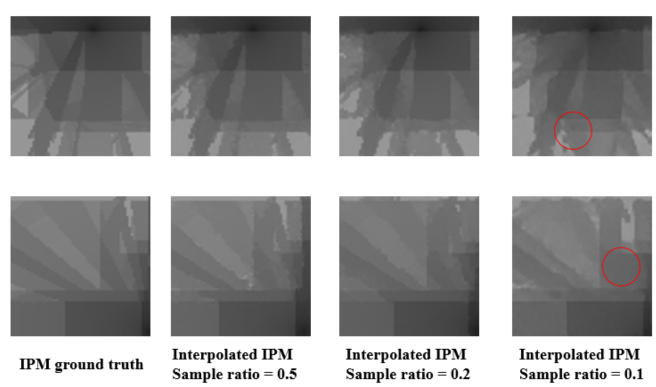

Fig. 5. Interpolation results generated by training the model from scratch using varying sample ratios for 2 scenarios.

Table 1 summarizes the results of these experiments, and Fig.5 visually depicts the interpolation results obtained with each sample ratio for the two scenarios shown on the upper and lower rows respectively.

TABLE I
RMSE RESULTS FOR IPMS HAVING DIFFERENT SAMPLE RATIOS

Sample Ratio	RMSE (dB)
0.1	5.19
0.2	3.67
0.5	2.54

Our study indicates that RDM can achieve high accuracy with relatively high sample ratios, demonstrating its efficacy and robustness in handling diverse datasets. Nonetheless, as the sample ratio decreases, the limitations of the RDM become more pronounced, as indicated by the red circles in the image shown in the final column of Fig.5. This is a result of the scarcity of RPs in a specific region because of random selection and low sample ratio. Moreover, decreasing the sample ratio leads to a substantial increase in training time. For example, training the RDM with a sample ratio of 0.1 requires twice the training time compared to training with a sample ratio of 0.2.

B. Multi-stage training

In order to enhance interpolation performance at lower sampling ratios and to minimize the training duration, a multi-stage training approach is proposed. Initially, the model is trained to employ a high sampling ratio, for instance, 0.5. Subsequently, the pre-trained model undergoes fine-tuning, with the sampling ratio being systematically reduced until the desired ratio of 0.1 is attained.

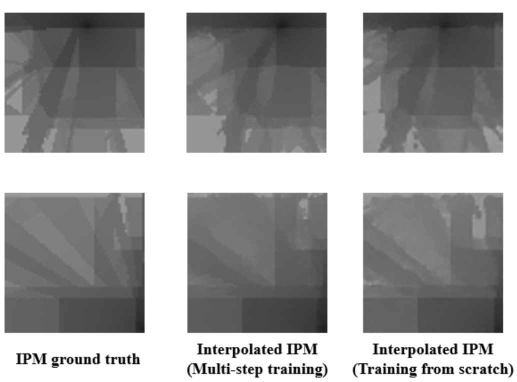

Fig. 6. Result of IPM interpolation using different training approaches.

Fig. 6 shows the interpolation results for two different scenarios with a 0.1 sampling ratio, highlighting the impact of different methods. The use of a multi-stage training approach led to a notable improvement in accuracy compared to starting the training from scratch. Specifically, an RMSE of 4.23dB was achieved, in contrast to the 5.19dB attained without employing the multi-stage training technique.

V. CONCLUSION

This paper introduces a groundbreaking RDM for accurate and reliable IPM interpolation with a limited number of RPs. This innovative approach effectively addresses the limitations of traditional interpolation methods in terms of accuracy and coverage area. A multi-stage training strategy is proposed to boost the model's performance and stability, which represents a significant advance in the field of IPM generation.

In addition to the novel RDM, the paper also presents a unique data processing pipeline along with a pre-processing technique that incorporates positional encoding with a Gaussian kernel and an online data augmentation method to enhance the training dataset and improve the generalization performance of the model, further differentiating it from existing approaches.

The evaluation results highlight the potential of this state-of-the-art approach to revolutionize the generation of IPMs for wireless network planning and deployment. While this paper presents a series of advances in IPM generation, it is important to acknowledge certain limitations introduced by the use of DDPM. Specifically, the requirement for a large number of refinement steps can make the process relatively slow, which could be a hindrance in time-sensitive applications. However, we are optimistic that ongoing research focused on accelerating generative models could mitigate this limitation. Future work will explore these avenues to further enhance the model's speed without compromising its performance, thereby continuing to advance the state-of-the-art in IPM generation for wireless network planning and deployment.

ACKNOWLEDGMENT

This work was supported by the European Commission through the Horizon 2020 Framework Program, H2020-MSCA-ITN-2019, MSCA-ITN-EID, under Grant 860239, BANYAN

References

[1] Y. B. Zikria, S. W. Kim, M. K. Afzal, H. Wang, and M. H. Rehmani, "5g mobile services and scenarios: Challenges and solutions," p. 3626, 2018.

[2] T. Kim Geok, K. Zar Aung, M. Sandar Aung, M. Thu Soe, A. Abdaziz, C. Pao Liew, F. Hossain, C. P. Tso, and W. H. Yong, "Review of indoor positioning: Radio wave technology," *Applied Sciences*, vol. 11, no. 1, p. 279, 2020.

[3] S. B. A. Khattak, M. Jia, Q. Guo, and X. Gu, "Improving positioning accuracy using wlan optimization for location based services and cognitive radio networks," in *International Conference on Wireless and Satellite Systems*. Springer, 2021, pp. 607–621.

[4] L. Zhang, Z. Chen, W. Cui, B. Li, C. Chen, Z. Cao, and K. Gao, "Wifi-based indoor robot positioning using deep fuzzy forests," *IEEE Internet of Things Journal*, vol. 7, no. 11, pp. 10 773–10 781, 2020.

[5] J. Racko, J. Machaj, and P. Brida, "Wi-fi fingerprint radio map creation by using interpolation," *Procedia engineering*, vol. 192, pp. 753–758, 2017.

[6] K. Suto, S. Bannai, K. Sato, K. Inage, K. Adachi, and T. Fujii, "Image-driven spatial interpolation with deep learning for radio map construction," *IEEE Wireless Communications Letters*, vol. 10, no. 6, pp. 1222–1226, 2021.

[7] S.-S. Jan, S.-J. Yeh, and Y.-W. Liu, "Received signal strength database interpolation by kriging for a wi-fi indoor positioning system," *Sensors*, vol. 15, no. 9, pp. 21 377–21 393, 2015.

[8] S. Ezpeleta, J. M. Claver, J. J. Pérez-Solano, and J. V. Martí, "Rf-based location using interpolation functions to reduce fingerprint mapping," *Sensors*, vol. 15, no. 10, pp. 27 322–27 340, 2015.

[9] Z. Yun and M. F. Iskander, "Ray tracing for radio propagation modeling: Principles and applications," *IEEE Access*, vol. 3, pp. 1089–1100, 2015.

[10] L. Azpilicueta, M. Rawat, K. Rawat, F. M. Ghannouchi, and F. Falcone, "A ray launching-neural network approach for radio wave propagation analysis in complex indoor environments," *IEEE Transactions on Antennas and Propagation*, vol. 62, no. 5, pp. 2777–2786, 2014.

[11] J. Thrane, D. Zibar, and H. L. Christiansen, "Model-aided deep learning method for path loss prediction in mobile communication systems at 2.6 ghz," *Ieee Access*, vol. 8, pp. 7925–7936, 2020.

[12] V. V. Ratnam, H. Chen, S. Pawar, B. Zhang, C. J. Zhang, Y.-J. Kim, S. Lee, M. Cho, and S.-R. Yoon, "Fadenet: Deep learning-based mm-wave large-scale channel fading prediction and its applications," *IEEE Access*, vol. 9, pp. 3278–3290, 2020.

[13] S. Bakirtzis, K. Qiu, J. Zhang, and I. Wassell, "Deepray: Deep learning meets ray-tracing," in *2022 16th European Conference on Antennas and Propagation (EuCAP)*. IEEE, 2022, pp. 1–5.

[14] L. Yang, Z. Zhang, Y. Song, S. Hong, R. Xu, Y. Zhao, Y. Shao, W. Zhang, B. Cui, and M.-H. Yang, "Diffusion models: A comprehensive survey of methods and applications," *arXiv preprint arXiv:2209.00796*, 2022.

[15] Ranplan Wireless Network Design, "Ranplan professional," https://www.ranplanwireless.com/gb/products/professional/, accessed 2023.

[16] H. Cao, C. Tan, Z. Gao, G. Chen, P.-A. Heng, and S. Z. Li, "A survey on generative diffusion model," *arXiv preprint arXiv:2209.02646*, 2022.

[17] J. Ho, A. Jain, and P. Abbeel, "Denoising diffusion probabilistic models," *Advances in Neural Information Processing Systems*, vol. 33, pp. 6840–6851, 2020.

[18] C. Saharia, J. Ho, W. Chan, T. Salimans, D. J. Fleet, and M. Norouzi, "Image super-resolution via iterative refinement," *IEEE Transactions on Pattern Analysis and Machine Intelligence*, 2022.

[19] C. Saharia, W. Chan, H. Chang, C. Lee, J. Ho, T. Salimans, D. Fleet, and M. Norouzi, "Palette: Image-to-image diffusion models," in *ACM SIGGRAPH 2022 Conference Proceedings*, 2022, pp. 1–10.

[20] K. Qiu, S. Bakirtzis, H. Song, J. Zhang, and I. Wassell, "Pseudo ray-tracing: Deep leaning assisted outdoor mm-wave path loss prediction," *IEEE Wireless Communications Letters*, vol. 11, no. 8, pp. 1699–1702, 2022.